Electronic Supplementary Material (ESI) for Journal of Materials Chemistry C.

Supporting Informations

Alternated bimetallic [Ru-M] (M = Fe^{2+}, Zn^{2+}) coordination polymers based on $[Ru(bpy)_3]^{2+}$ units connected to bis-terpyridine ligands : synthesis, electrochemistry and photophysics in solution or in thin film on electrodes.

Jean Lombard,[a] D. Amilan Jose,[a] Carmen E. Castillo,[a] Robert Pansu,[b] Jérôme Chauvin,[a*] Alain Deronzier,[a*] Marie-Noëlle Collomb[a*]

[a] Université Grenoble Alpes, DCM, F-38000 Grenoble, France CNRS, DCM, F-38000 Grenoble, France
E-mail: jerome.chauvin@ujf-grenoble.fr; alain.deronzier@ujf-grenoble.fr; marie-noelle.collomb@ujf-grenoble.fr
[b] Ecole Normale supérieure de Cachan / CNRS, Laboratoire de Photophysique et Photochimie Supramoléculaire et Macromoléculaires, UMR-8531, 61 av. du Président Wilson, 94235 Cachan Cedex, France

1- Mass Spectroscopies of $[\{Ru^{II}\text{-}Fe^{II}\}_n]^{4n+}$

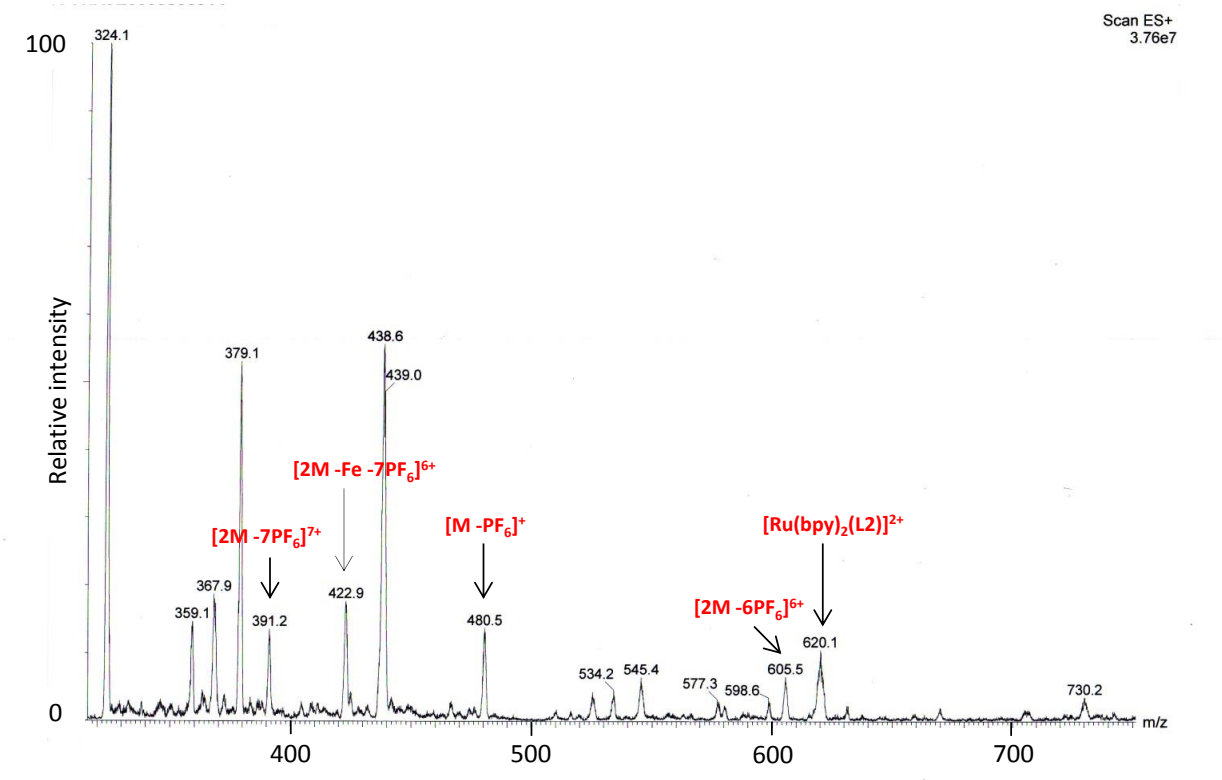

Figure SI1: ESI-MS of the polymer $[\{Ru^{II}\text{-}Fe^{II}\}_n](PF_6)_{4n}$, M corresponds to the monomer structure, M = $[Ru(bpy)_2(L2)Fe](PF_6)_4$.

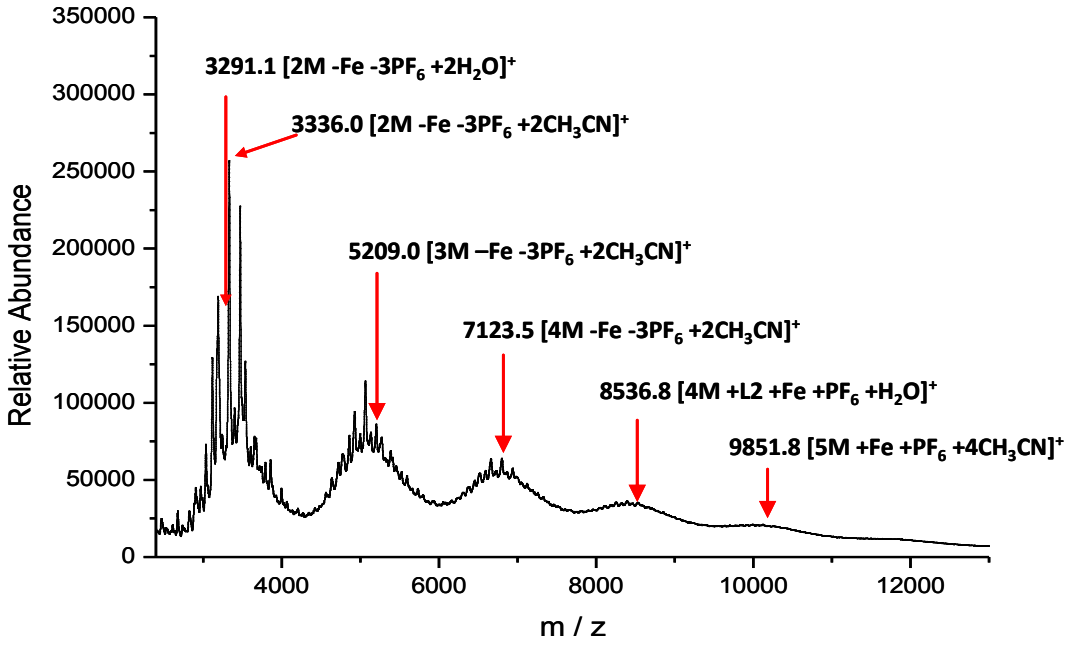

Figure SI2: Partial MALDI-TOF mass spectrum of the polymer $[\{Ru^{II}\text{-}Fe^{II}\}_n](PF_6)_{4n}$ (M refers to the monomer structure, M = $[Ru(bpy)_2(L2)Fe](PF_6)_4$)). The spectrum was measured in the positive-ion mode using 2,5-dihydroxbenzoic acid as the matrix and acetonitrile as the solvent.

2-Electrochemical behaviour of $[Ru(bpy)_2L2]^{2+}$ (B).

The reversible metal-based oxidation process, Ru^{III}/Ru^{II}, appears at $E_{1/2}$ = +0.92 V (eq. 1) (Figure SI1 and Table SI1). Three successive ligand-centered reduction processes are observed in the negative potential region. These systems can be attributed by comparison with the electroactivity of $[Ru^{II}(bpy)_3]^{2+}$ to the two first the one-electron reduction of the bipyridine ligands (eqs (2-3)) ; the third one is due to bipyridine ligand bearing the two terpyridine (eq. (4)).

$[Ru^{II}(bpy)_2(tpy\text{-}bpy\text{-}tpy)]^{2+} \rightleftarrows [Ru^{III}(bpy)_2(tpy\text{-}bpy\text{-}tpy)]^{3+} + 1e^-$ (1)

$[Ru^{II}(bpy)_2(tpy\text{-}bpy\text{-}tpy)]^{2+} + 1e^- \rightleftarrows [Ru^{II}(bpy^{\cdot -})(bpy)(tpy\text{-}bpy\text{-}tpy)]^{+}$ (2)

$[Ru^{II}(bpy^{\cdot -})(bpy)(tpy\text{-}bpy\text{-}tpy)]^{+} + 1e^- \rightleftarrows [Ru^{II}(bpy^{\cdot -})_2(tpy\text{-}bpy\text{-}tpy)]^{+}$ (3)

$[Ru^{II}(bpy^{\cdot -})_2(tpy\text{-}bpy\text{-}tpy)]^{+} + 1e^- \rightleftarrows [Ru^{II}(bpy^{\cdot -})_2(tpy\text{-}bpy^{\cdot -}\text{-}tpy)]^{+}$ (4)

In contrast to $[Ru^{II}(bpy)_2(L1)]^{2+}$, which exhibits four successive one-electron reversible waves,[1] some adsorption phenomena coupled to the second reduction process for $[Ru^{II}(bpy)_2(L2)]^{2+}$ leads to an important distortion of this second system on the reverse scan as well as the third ligand reduction wave, due to redissolution phenomena. The adsorption phenomena is due to the formation of the neutral species $[Ru^{II}(bpy^{\bullet -})_2(tpy\text{-}bpy\text{-}tpy)]^0$ (eq (3)) followed by its

electrodepostion at the electrode surface and by its desorption either by reoxydation during the reverse scan (sharp reoxydation peak), nor by scanning at more negative potential including the third reduction process (sharp reduction peak).

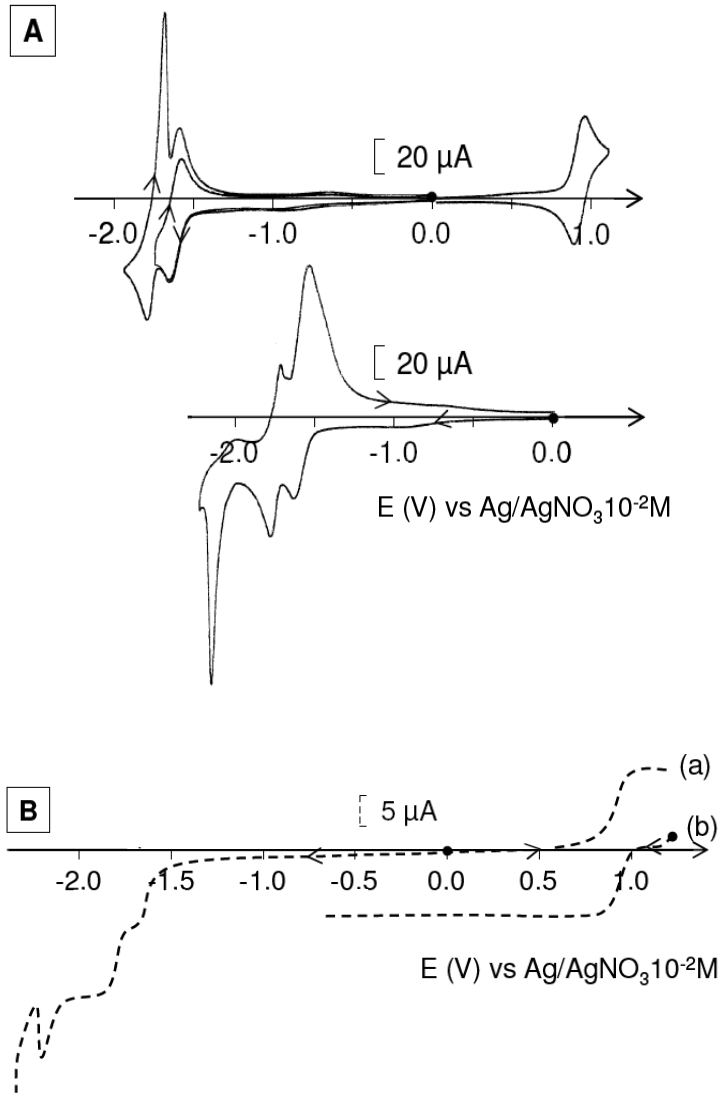

Figure SI3: (A) Cyclic voltammograms in CH_3CN + 0.1M $[Bu_4N]ClO_4$ at a Pt working electrode of a 0.96 mM solution of $[Ru^{II}(bpy)_2(L2)]^{2+}$, v = 100mV s^{-1}. (B) Voltammograms at a rotating disk electrode (RDE) of the same solution at a Pt electrode, ω = 600 tr min^{-1}, v = 10 mV s^{-1}: (a) initial solution, (b) after exhaustive electrolysis at + 1.10 V

The stability of $[Ru^{III}(bpy)_2(L2)]^{3+}$ has been evaluated by an exhaustive electrolysis at +1.10 V. After exhaustive electrolysis (one electron exchange), the typical MLCT absorption band of the Ru^{II} at 455 nm disappears and is replaced by the lower intensity Ru(III) bands at 430 and 660 nm. The Ru^{III} species is formed with a 90% yield as evidenced by rotation disk electrode experiments (Figure SI1B).

Table SI1: Redox potentials of $[Ru^{II}(bpy)_2(L1)]^{2+}$ and $[Ru^{II}(bpy)_2(L2)]^{2+}$ in deoxygenated CH_3CN + 0.1 M Bu_4NClO_4 at a scan rate of 100 mV s^{-1}. $E_{1/2}$(V) (ΔEp/mV) vs Ag/Ag^+ ($AgNO_3$ 0.01 M in CH_3CN + 0.1 M Bu_4NClO_4)

Complexes	Oxidation processes	Reduction processes (ligand centered)				
	Ru^{II}/Ru^{III}	1	2	3	4	5
$[Ru^{II}(bpy)_2(L1)]^{2+,1}$	0.94 (70)	-1.67 (60)	-1.87 (70)	-2.13 (70)	-2.37 (80)	-2.60[a] (100)
$[Ru^{II}(bpy)_2(L2)]^{2+,}$	0.92 (70)	-1.67 (60)	-1.87 (70)	-2.19[b] (100)		

[a] This value cannot be accurately determined due to the proximity of the solvent reduction.
[b]This value cannot be accurately measured since the wave is strongly distorted by adsorption of the reduction product on the electrode surface.

2-Electrochemical behavior of $[\{Ru^{II}\text{-}Fe^{II}\}_n]^{4n+}$ and $[\{Ru^{II}\text{-}Zn^{II}\}_n]^{4n+}$

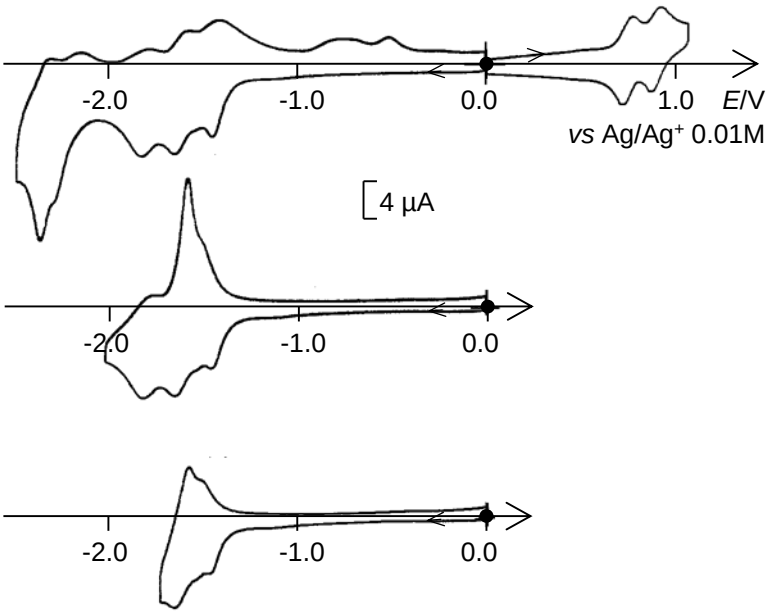

Figure SI4: Cyclic voltammograms in in CH_3CN + 0.1M $[Bu_4N]ClO_4$ at a vitreous carbon working electrode of a 0.24 mM solution of $[\{Ru^{II}\text{-}Fe^{II}\}_n]^{4n+}$; scan rate: 100 mV s^{-1}.

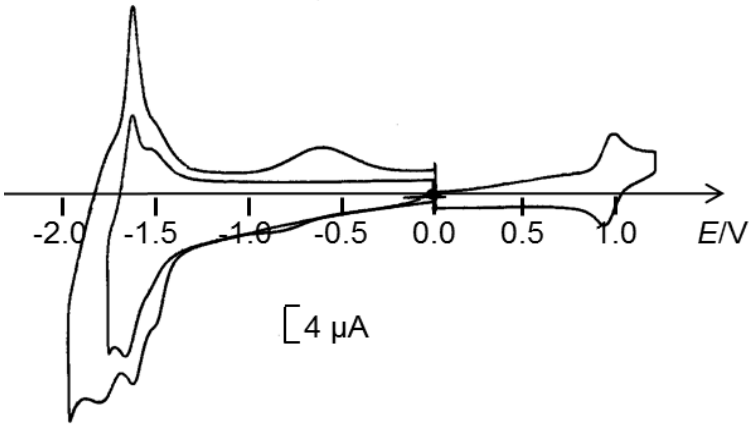

Figure SI5: Cyclic voltammograms in CH_3CN + 0.1M $[Bu_4N]ClO_4$ at a Pt working electrode of a 0.25 mM solution of $[\{Ru^{II}\text{-}Zn^{II}\}_n]^{4n+}$; scan rate: 100 mV s^{-1}.

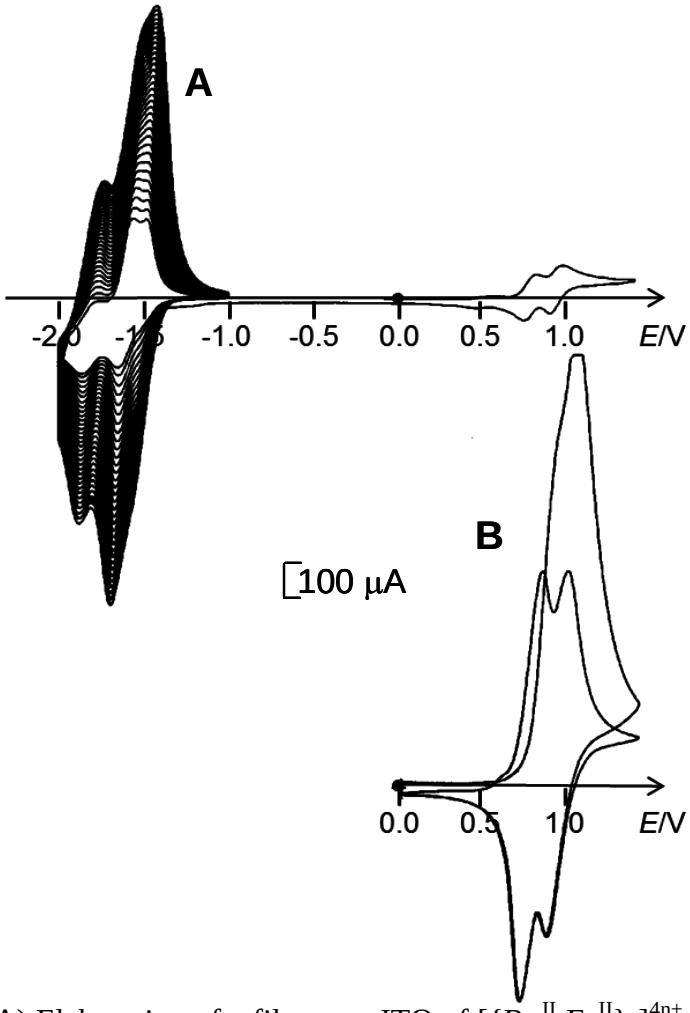

Figure SI6: (A) Elaboration of a film over ITO of $[\{Ru^{II}\text{-}Fe^{II}\}_n]^{4n+}$ by successive potential scans between 0 and -2.0 V from a solution of $[\{Ru^{II}\text{-}Fe^{II}\}_n]^{4n+}$ (1.1 mM) in CH_3CN + 0.1 M $[Bu_4N]ClO_4$, (B) Cyclic voltammograms of the resulting ITO/$[\{Ru^{II}\text{-}Fe^{II}\}_n]^{4n+}$ film prepared in (A) after transfer in CH_3CN + 0.1 M $[Bu_4N]ClO_4$ ($\Gamma = 5.83 \times 10^{-8}$ mol/cm^2); scan rate 50 mV s^{-1}.

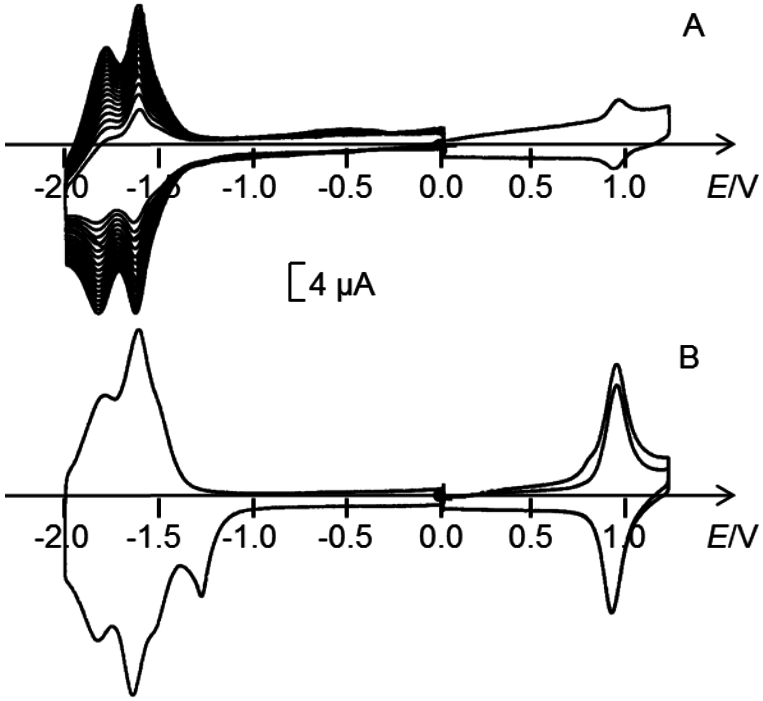

Figure SI7: (A) Elaboration of a modified electrode C/[{Ru^{II}-Zn^{II}}$_n$]$^{4n+}$ by successive potential scans between 0 and -2.0 V from a solution of [{Ru^{II}-Zn^{II}}$_n$]$^{4n+}$ (0.25 mM) in CH_3CN + 0.1 M $[Bu_4N]ClO_4$, (B) CV of the modified electrode prepared in (A) after transfer in CH_3CN + 0.1 M $[Bu_4N]ClO_4$ scan rate 100 mV s^{-1}.

3-Absorption and emission properties of [{Ru^{II}-Zn^{II}}$_n$]$^{4n+}$ on ITO electrode

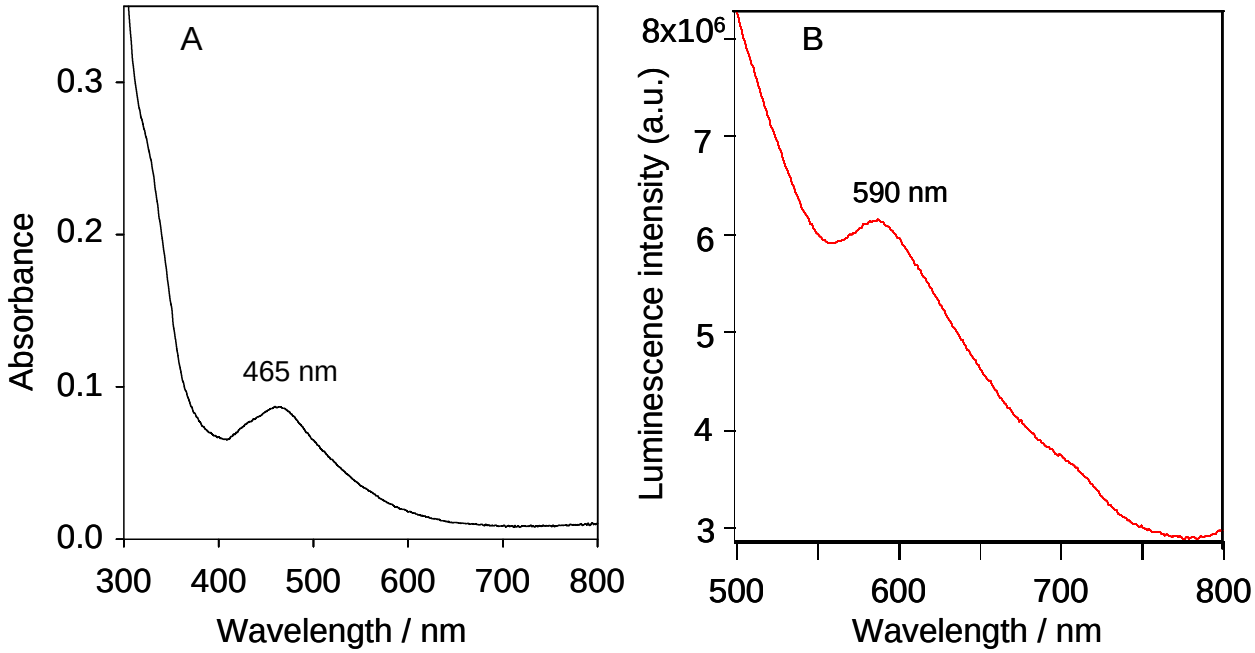

Figure SI8: UV-Vis (A) and emission (B) spectra of [{Ru^{II}-Zn^{II}}$_n$]$^{4n+}$ electro-deposited on ITO (Γ = 3.91 $\times 10^{-8}$ mol/cm^2).

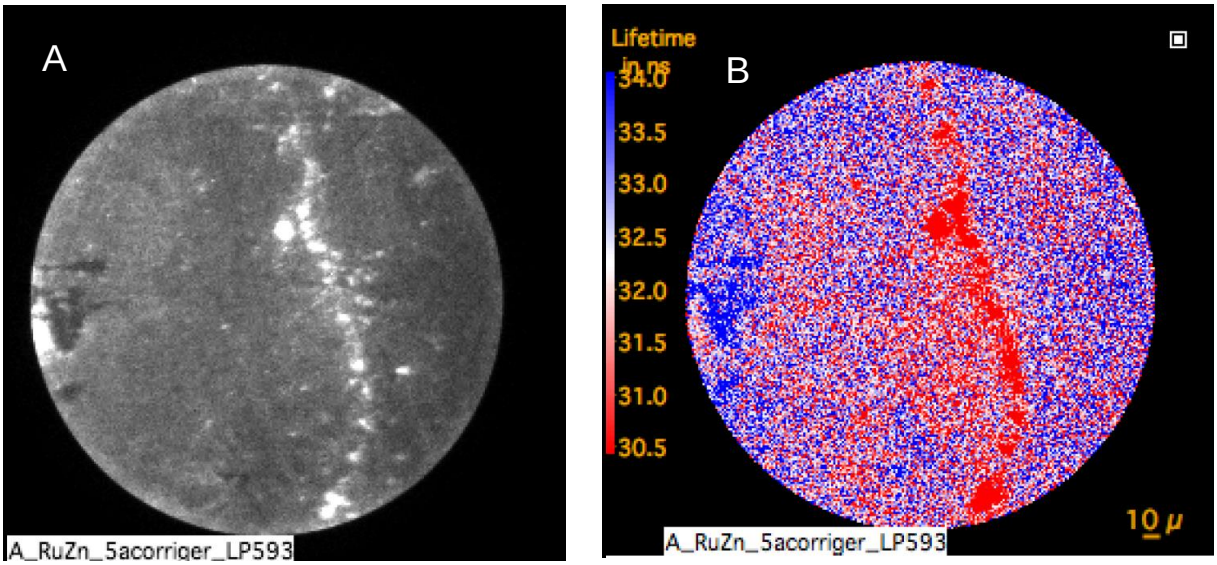

Figure SI9 : Emission properties of a $[\{Ru^{II}\text{-}Zn^{II}\}_n]^{4n+}$ film on ITO (Γ = 4.02 $\times 10^{-8}$ mol/cm^2) recorded upon excitation at 343 nm. (A) Steady state emission and (B) Emission decay map.

Reference:

[1] J. Lombard, J.-C. Lepretre, J. Chauvin, M.-N. Collomb, A. Deronzier, *Dalton Trans.* 2008, 658-666.